

Optimizing Piezoelectric Panel Speakers Using Simulated Annealing Algorithm

Mingsian R. Bai (1), Yao Kun Tsai (2)

(1) Department of Mechanical Engineering, National Chiao-Tung University, 1001 Ta-Hsueh Road, Hsin-Chu 300, Taiwan.

(2) Department of Mechanical Engineering, National Chiao-Tung University, 1001 Ta-Hsueh Road, Hsin-Chu 300, Taiwan

PACS: 43.38.Bs, 43.38.Ja, 43.40.Dx.

ABSTRACT

This paper is focused on optimization of piezoelectric panel speakers. Two piezoelectric ceramic plates serve to excite the diaphragm in the speaker. With the optimization procedure, the best position to mount piezoelectric ceramic plates on the diaphragm is determined. A finite element model is established using the energy method, where the electrical system, mechanical system and acoustic loading of the transducer are considered as a coupled system. The simulated annealing (SA) algorithm is exploited to attain low fundamental resonance frequency and high the acoustic output. Experiments were conducted to verify the numerical model. The experimental results were in good agreement with the numerical prediction. The performance of the optimized configuration was significantly improved over the non-optimal design.

INTRODUCTION

Recently, miniaturized loudspeakers have been extensively studied owing to the rapid growth of consumer electronics. The major challenge of the components in consumer electronics is how to reduce their sizes without compromising the performance. For example, for laptop computers bundled with CULV (Consumer Ultra Low Voltage) processors and handheld devices, the traditional loudspeakers usually fail to fulfill the space or thickness constraints. These physical limitations hence motivate the present study of an alternative design using piezoelectric panel speakers.

Piezoelectric materials have found applications in many areas of sensors and actuators since the discovery of piezoelectricity by Curie brothers [1] a century ago. However, it was not until recently people started to explore the possibility of using it as driving mechanism for panel speakers, e.g., Taiyo Yudan [2], Murata [3], NXT [4], etc. One advantage of such device is that the electroacoustic efficiency of piezoelectric materials is considerably higher than their voice-coil counterpart, which is an appealing feature for battery driven products.

Lee and White [5] applied additional layers onto cantilever acoustic device to reduce the fundamental frequency and improve acoustic output. Woodard [6] used tailoring vibration response, vibration topography, acoustic chamber and tailoring damping to improve the acoustic performance. Chu *et al.* [7] optimized the shape of piezoelectric plate to reduce the fundamental frequency. Various approaches such as the genetic algorithm and Taguchi method dealing with optimal design were reported in literature [8-10]. Improving

acoustic output at lower frequency becomes the common topic in piezoelectric speakers design.

In this paper, a new configuration of piezoelectric panel speaker in conjunction with simulated annealing [11] (SA) algorithm is proposed to optimize the piezoelectric speakers design. Instead of directly applying the piezoelectric ceramic plates on the diaphragm, we use two cantilever piezoelectric ceramic plates clamped at a surrounding frame. Spacers are inserted between the piezoelectric ceramic plates and the diaphragm through which forces are transmitted to the diaphragm. For this piezoelectric panel speaker, a finite element model was developed in the paper to serve as the basis of design optimization. The energy method is employed to establish the dynamic model of the piezoelectric speaker. Acoustic loading is accounted for during the modeling stage because of its light diaphragm structure. With the numerical model, optimization based on the simulated annealing (SA) algorithm is carried out to reach the best compromise between the fundamental frequency and acoustic output. The outcome of the optimization procedure is the best position to deploy the piezoelectric ceramic plates.

MODELLING OF PIEZOELECTRIC PANEL SPEAKER

The energy method in conjunction with the finite element method (FEM) is employed to derive the equations of motion for the coupled electrical and mechanical systems. The radiation loading is taken into account in light of the Rayleigh's integral.

Finite element model

The loudspeaker structure under study is shown in Fig. 1. It consists of a diaphragm, a pair of piezoelectric ceramic plates and a pair of spacers.

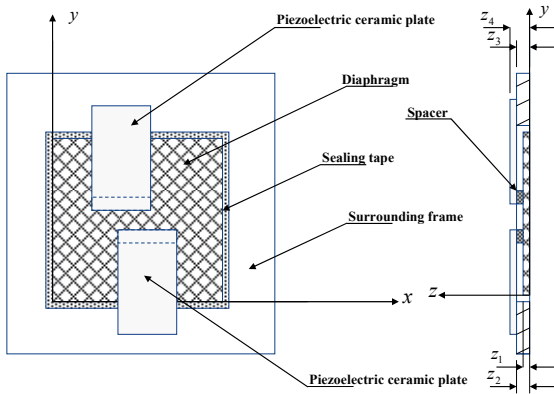


Figure 1. Schematic diagram of the piezoelectric panel speaker.

Finite element analysis (FEA) is employed to model these components. The lateral displacement w is interpolated by cubic polynomials of physical coordinates [12]

$$w = Nd, \tag{1}$$

where

$$d = [w_1, \theta_1, \phi_1, w_2, \theta_2, \phi_2, w_3, \theta_3, \phi_3, w_4, \theta_4, \phi_4]^T,$$

N denotes row vector of shape functions. The degrees of freedom (dof) of each node (i) consists of one lateral deflection w_i , rotation $\partial w_i / \partial x = \theta_i$ and $\partial w_i / \partial y = \phi_i$, $i = 1, 2, 3, 4$, as shown in Fig. 2.

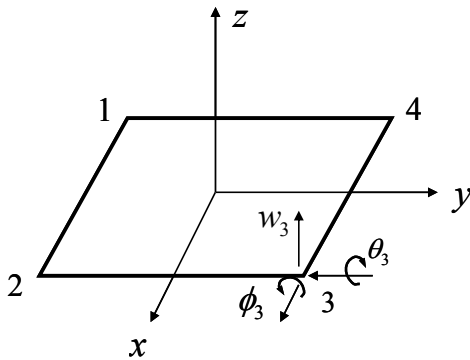
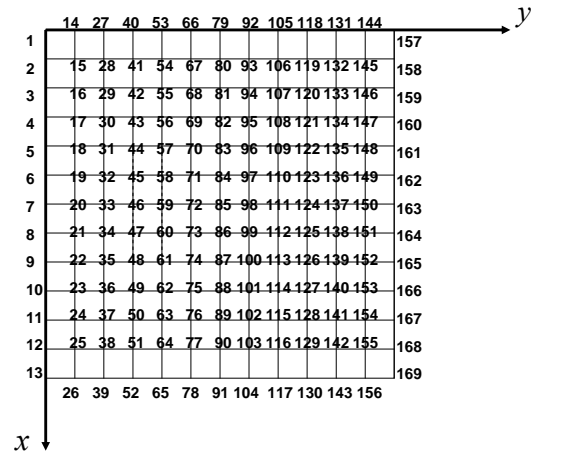
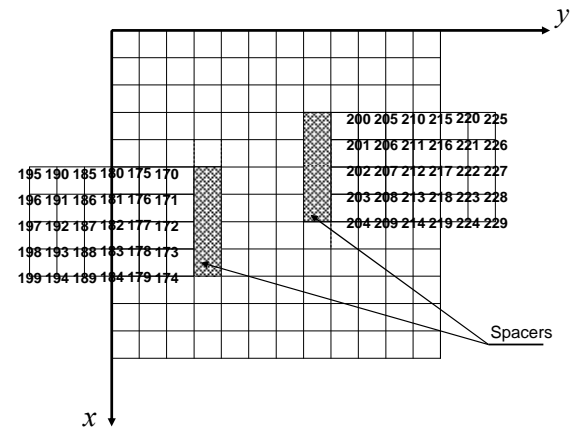


Figure 2. 12-dof rectangular Kirchhoff plate element with dofs indicated at node 3.

The mesh configuration is shown in Figs. 3(a) and (b).



(a)



(b)

Figure 3. FEM mesh structure for modeling the piezoelectric panel speaker. (a) Complete mesh with 144 elements for diaphragm. (b) Complete mesh with 56 elements for piezoelectric ceramic plates.

The generalized Hamilton principle has the following form

$$\delta \int_{t_1}^{t_2} L(w, w_t, t) dt = 0, \tag{2}$$

where

$$L = \Gamma - U, \tag{3}$$

Γ and U are the kinetic energy and generalized potential energy defined as

$$\Gamma = \frac{1}{2} \int_{S_p} \rho_p w_{tt} dS + \frac{1}{2} \int_{S_z} \rho_z w_{tt} dS + \frac{1}{2} \int_{S_s} \rho_s w_{tt} dS, \tag{4}$$

$$U = \int_{V_z} \Phi dV + \int_{S_p} U_p dS + \int_{S_s} U_s dS, \tag{5}$$

where ρ_p , ρ_z , and ρ_s are the area densities of the diaphragm, piezoelectric ceramic plates and spacers, respectively. S_p , S_z , and S_s are the areas of the diaphragm, piezoelectric ceramic plates and spacers, respectively. q is the electric charge on the electrodes. The subscript “ tt ” symbolizes the second partial derivative with respect to time t ; similar rule applies to

the other variables. Φ denotes the potential energy of the piezoelectric ceramic plates and can be written as a quadratic form

$$\Phi = \frac{1}{2} \mathbf{S}^T \mathbf{cS} - \frac{1}{2} \mathbf{E}^T \boldsymbol{\varepsilon} \mathbf{E} - \mathbf{S}^T \mathbf{e} \mathbf{E}, \quad (6)$$

where \mathbf{S} and \mathbf{E} are the vectors of the strain and electrical field. \mathbf{c} , \mathbf{e} , and $\boldsymbol{\varepsilon}$ are the matrices of elastic, piezoelectric, and dielectric constants. The bending strain energy of the diaphragm and the spacer is given by

$$U_P = w_{xx}^2 + w_{yy}^2 + 2\nu w_{xx} w_{yy} + 2(1-\nu_P) w_{xy}^2, \\ U_S = w_{xx}^2 + w_{yy}^2 + 2\nu w_{xx} w_{yy} + 2(1-\nu_S) w_{xy}^2, \quad (7)$$

where ν_P and ν_S are the Poisson's ratios of the diaphragm and the spacer, respectively. Substituting Eqs. (1), (4) and (5) into Eq. (2) yields the global finite-element equations:

$$\mathbf{M}\ddot{\mathbf{D}} + \mathbf{C}\dot{\mathbf{D}} + \mathbf{K}\mathbf{D} + \boldsymbol{\eta}\mathbf{q} = \mathbf{f}, \quad (8)$$

$$\boldsymbol{\eta}^T \mathbf{D} + \zeta \mathbf{q} = \mathbf{v}, \quad (9)$$

\mathbf{D} is the vector of global degree of freedom. \mathbf{f} and \mathbf{v} are non-inertia forces and can be derived in light of the principle of virtual work. The other matrices and vectors are given by

$$\mathbf{M} = \sum_{i=1}^{s_1} \rho_P \int_{S_{Pe}} \mathbf{N}^T \mathbf{N} dS + \sum_{j=1}^{s_2} \rho_Z \int_{S_{Ze}} \mathbf{N}^T \mathbf{N} dS + \sum_{k=1}^{s_3} \rho_S \int_{S_{Se}} \mathbf{N}^T \mathbf{N} dS \quad (10)$$

$$\mathbf{K} = \mathbf{K}_Z + \mathbf{K}_P + \mathbf{K}_S, \quad (11)$$

$$\mathbf{K}_Z = \sum_{i=1}^{s_2} -2a_1 \int_{S_{Ze}} \mathbf{N}_{xy}^T \mathbf{N}_{xy} dS + 2a_2 \int_{S_{Ze}} \mathbf{N}_{xx}^T \mathbf{N}_{xx} dx \quad (12)$$

$$+ 2a_3 \int_{S_{Ze}} \mathbf{N}_{yy}^T \mathbf{N}_{yy} dS + 2a_4 \int_{S_{Ze}} \mathbf{N}_{xx}^T \mathbf{N}_{yy} dS \\ \mathbf{K}_P = \sum_{j=1}^{s_1} \int_{S_{Pe}} \begin{bmatrix} \mathbf{N}_{xx} & \mathbf{N}_{yy} & 2\mathbf{N}_{xy} \\ D_p & v_P D_p & 0 \\ v_P D_p & D_p & 0 \\ 0 & 0 & (1-\nu_P) D_p / 2 \end{bmatrix} \begin{bmatrix} \mathbf{N}_{xx}^T \\ \mathbf{N}_{yy}^T \\ 2\mathbf{N}_{xy}^T \end{bmatrix} dS \quad (13)$$

$$\mathbf{K}_S = \sum_{k=1}^{s_3} \int_{S_{Se}} \begin{bmatrix} \mathbf{N}_{xx} & \mathbf{N}_{yy} & 2\mathbf{N}_{xy} \\ D_S & \nu_S D_S & 0 \\ \nu_S D_S & D_S & 0 \\ 0 & 0 & (1-\nu_S) D_S / 2 \end{bmatrix} \begin{bmatrix} \mathbf{N}_{xx}^T \\ \mathbf{N}_{yy}^T \\ 2\mathbf{N}_{xy}^T \end{bmatrix} dS \quad (14)$$

$$\boldsymbol{\eta} = a_5 \sum_{i=1}^m \int_{S_{Ze}} (\mathbf{N}_{xx}^T + \mathbf{N}_{yy}^T) dS, \quad (15)$$

$$\zeta = a_6, \quad (16)$$

$$\mathbf{v} = \frac{1}{S_Z} \sum_{i=1}^m \int_{S_{Ze}} v_z(t) dS, \quad (17)$$

$$a_1 = 2c_{66}^D (z_4^3 - z_3^3) / 3, a_2 = c_{11}^D (z_4^3 - z_3^3) / 6, \\ a_3 = c_{11}^D (z_4^3 - z_3^3) / 6, a_4 = c_{12}^D (z_4^3 - z_3^3) / 3, \\ a_5 = h_{31} (z_4^2 - z_3^2) / 2S_{Ze}, a_6 = \beta_{33} (z_4 - z_3) / S_{Ze}, \quad (18)$$

where s_1 , s_2 and s_3 are the total number of elements for diaphragm, piezoelectric ceramic plates and spacers, respectively.

$$D_P = \frac{E_P z_1^3}{12(1-\nu_P^2)} \quad \text{and} \quad D_S = \frac{E_S (z_2^3 - z_1^3)}{12(1-\nu_S^2)}$$

are bending stiffness of the diaphragm and the spacer, respectively, z_1 is the thickness of the diaphragm, z_2 is the stacking thickness of diaphragm and spacer. S_{Pe} , S_{Ze} , and S_{Se} are the area of each element of the diaphragm, piezoelectric ceramic plates and spacers, respectively. E_P and E_S are the Young's modulus of the diaphragm and the spacer, respectively. h is the piezoelectric voltage constant, c^D is the elastic stiffness under the condition of constant electric displacement, β^S is the permittivity under the condition of constant strain, and the subscripts signify the orientation and mechanical quantities.

\mathbf{C} is assumed as the proportional damping [14] in this paper for simplicity, i.e., the damping matrix

$$\mathbf{C} = \alpha \zeta \mathbf{M} + \beta (\zeta \mathbf{K} - \boldsymbol{\eta} \boldsymbol{\eta}^T), \quad (19)$$

where α and β are constants.

Radiation Impedance

Let \mathbf{p} and \mathbf{v} be the pressure vector and the velocity vector measured at discrete points on the surface of the structure. \mathbf{p} and \mathbf{v} are related by a radiation impedance matrix \mathbf{Z} [13]

$$\mathbf{p} = \mathbf{Z} \mathbf{v}. \quad (20)$$

For a baffled planar radiator, the matrix \mathbf{Z} can be approximated by a discrete Rayleigh's integral as

$$\mathbf{Z} = \rho_a c_s \begin{bmatrix} 1 - e^{-jk\sqrt{A_e}/\pi} & \frac{jkA_e}{2\pi} e^{-jk r_{12}} & \dots & \frac{jkA_e}{2\pi} e^{-jk r_{1n}} \\ \frac{jkA_e}{2\pi} e^{-jk r_{21}} & 1 - e^{-jk\sqrt{A_e}/\pi} & \dots & \vdots \\ \vdots & \vdots & \ddots & \vdots \\ \frac{jkA_e}{2\pi} e^{-jk r_{m1}} & \dots & \dots & 1 - e^{-jk\sqrt{A_e}/\pi} \end{bmatrix}, \quad (21)$$

where ρ_a is the air density, c_s is the sound speed, k is the wave number, r_{mn} is the distance between the nodes m and n ($r_{mn} = r_{nm}$, $1 \leq m, n \leq N$). Therefore, the external force vector \mathbf{f} is simply the pressure multiplied by the effective element area A_e

$$\mathbf{f} = A_e \mathbf{p} = A_e \mathbf{Z} \mathbf{v} = j\omega A_e \mathbf{Z} \mathbf{D}. \quad (22)$$

Incorporating the damping matrix \mathbf{C} and the external force vector \mathbf{f} into Eq. (8) enables rewriting the displacement vector \mathbf{D} as

$$\mathbf{D} = [\zeta (\mathbf{M} \omega^2 - \mathbf{K} - j\omega \mathbf{C} + j\omega A_e \mathbf{Z}) + \boldsymbol{\eta} \boldsymbol{\eta}^T]^{-1} \boldsymbol{\eta} \mathbf{v}. \quad (23)$$

Radiated sound pressure

Now that the surface displacements have been obtained from Eq. (23), the radiated sound pressure at a field point can be calculated using the following matrix equation [13]

$$\mathbf{p}_f = \mathbf{E}\mathbf{v}, \quad (24)$$

where \mathbf{p}_f is the radiated sound pressure vector, \mathbf{v} is the surface velocity vector that can be calculated by differentiating displacements in Eq. (23), and \mathbf{E} is the propagation matrix. For a baffled planar radiator, the propagation matrix \mathbf{E} can be approximated as

$$\mathbf{E} = j \frac{\rho_a c_s k A_e}{2\pi} \begin{bmatrix} \frac{e^{-jkr_{11}}}{r_{11}} & \frac{e^{-jkr_{12}}}{r_{12}} & \dots & \frac{e^{-jkr_{1n}}}{r_{1n}} \\ \frac{e^{-jkr_{21}}}{r_{21}} & \frac{e^{-jkr_{22}}}{r_{22}} & \dots & \frac{e^{-jkr_{2n}}}{r_{2n}} \\ \vdots & \vdots & \ddots & \vdots \\ \frac{e^{-jkr_{m1}}}{r_{m1}} & \frac{e^{-jkr_{m2}}}{r_{m2}} & \dots & \frac{e^{-jkr_{mn}}}{r_{mn}} \end{bmatrix}, \quad (25)$$

where r_{mn} is the distance between the center of the element n and the field point m .

OPTIMAL DESIGN OF PIEZOELECTRIC PANEL SPEAKER

Simulated annealing algorithm

Simulated annealing (SA) algorithm is a global optimization technique based on the notion resembling the annealing process of metallurgy. Given a cost function $J(\mathbf{e})$ defined as the function of the design parameter vector $\mathbf{e} = \mathbf{e}(e_1, e_2, \dots, e_n)$ is to be maximized, the SA procedure can be summarized as follows:

- 1) Choose initial temperature T_0 and \mathbf{e}_i , and specify the annealing schedule.
- 2) Evaluate $J(\mathbf{e}_i)$.
- 3) Perturb \mathbf{e}_i to obtain neighboring parameters \mathbf{e}_{i+1} and evaluate $J(\mathbf{e}_{i+1})$.
- 4) If $J(\mathbf{e}_{i+1}) \geq J(\mathbf{e}_i)$, \mathbf{e}_{i+1} is updated as the current solution.
- 5) If $J(\mathbf{e}_{i+1}) < J(\mathbf{e}_i)$, then accept \mathbf{e}_{i+1} as the current solution if $\exp(-\Delta/T) > \tau$, where $\Delta = J(\mathbf{e}_{i+1}) - J(\mathbf{e}_i)$ and τ is a random number following the uniform distribution in the interval $[0, 1]$; otherwise go to step 3.
- 6) Reduce the temperature if the number of iterations meet cooling schedule, otherwise go to step 3.
- 7) Terminate the algorithm if $T \leq T_f$; otherwise go to step 3.

In the context of the piezoelectric panel speaker design, the cost function we wish to maximize is

$$J = \frac{10^{(p_{avg}-94)/20}}{f_0} \times 10^4, \quad (26)$$

where the f_0 is the first resonance frequency with the sound pressure level greater than 40 dB, the p_{avg} is an average of the magnitude of sound pressure level in dB above the frequency f_0 . Our goal of the SA optimization is to minimize the fundamental frequency f_0 and to maximize the average sound pressure level p_{avg} in the bandwidth 20 Hz to 8 kHz, as shown in Fig. 4.

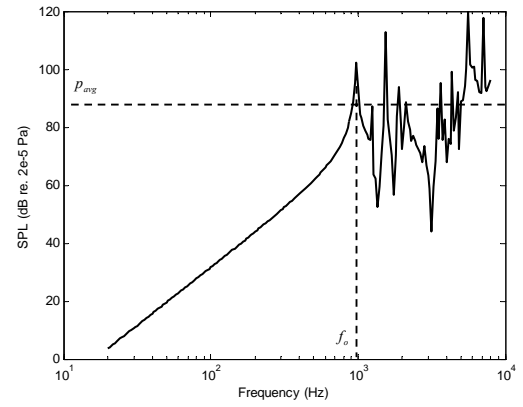


Figure 4. On-axis SPL response of a piezoelectric panel speaker. f_0 is the fundamental frequency greater than 40 dB, and p_{avg} is average SPL from f_0 to 8 kHz.

Annealing Schedule

The annealing schedule is crucial to the search performance in that it determines the degree of uphill movement during the search. To be specific, the following parameters need be specified in the annealing schedule:

- a) An initial temperature T_0 .
- b) Final temperature T_f or a stopping criterion.
- c) Length for the Markov chains [11].
- d) Rule for decrementing the temperature, e.g., $T_{i+1} = \alpha_T T_i$ with α_T being the annealing coefficient.

Fig. 5 depicts an SA flow chart for optimizing piezoelectric speaker parameters.

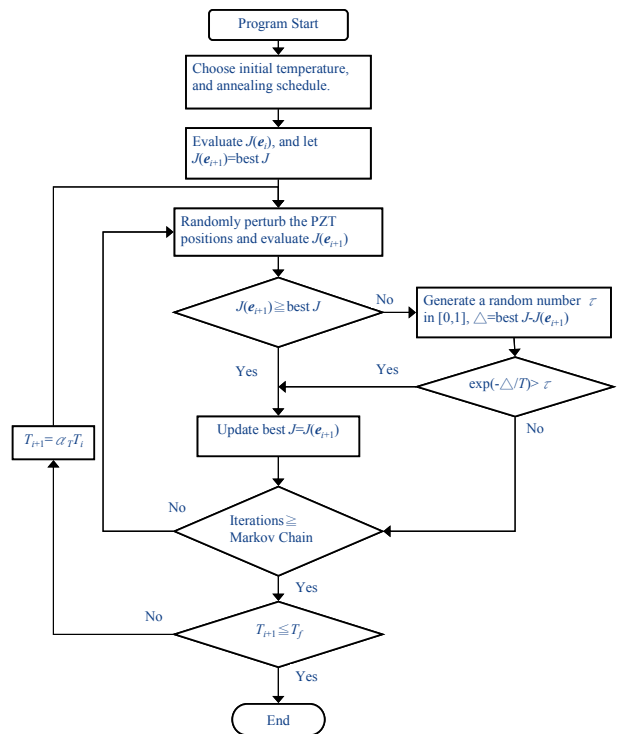


Figure 5. Flowchart of the SA optimization procedure

The data of the piezoelectric ceramic plates, the spacer and the diaphragm in our simulation are shown in Table 1.

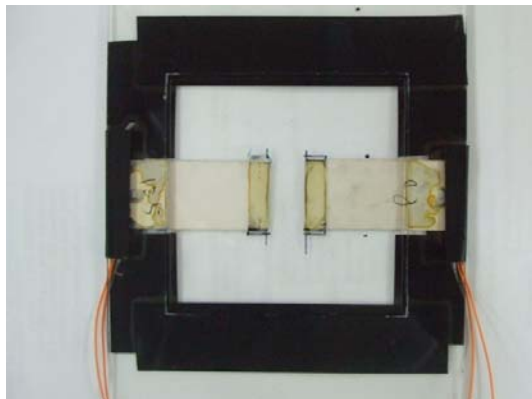
Table 1. The parameters of the piezoelectric ceramic plates, the diaphragm and the spacer used in the simulation and experiments.

	Material	Parameter	Value
Diaphragm	PC	size	0.06 m × 0.06 m × 0.000254 m
		density	1200 kg/m ³
		Young's modulus	7 GPa
		Poisson's ratio	0.37
Spacer	PC	size	0.005 m × 0.035 m × 0.000254 m
		density	1200 kg/m ³
		Young's modulus	7 GPa
		Poisson's ratio	0.37
Piezoelectric ceramic plate	PZT	size	0.02 m × 0.035 m × 0.002 m
		density	7800 kg/m ³
		β_{33}^s	3.52×10^7
		h_{31}	-3.6772×10^8 V/m
		c_{11}^D	12.236×10^{10} N/m ²
		c_{12}^D	5.244×10^{10} N/m ²
		c_{66}^D	3.496×10^{10} N/m ²

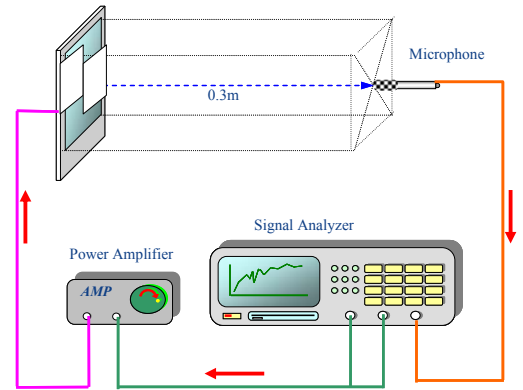
The piezoelectric ceramic plates are made of lead zirconate titanate (PZT). The diaphragm and spacers are made of polycarbonate (PC) with hard coat. The positions to mount the piezoelectric ceramic plates are determined using the preceding SA optimization procedure such that minimal fundamental frequency and maximal acoustic output can be achieved.

NUMERICAL SIMULATIONS AND EXPERIMENTAL INVESTIGATIONS

The prototype of the proposed piezoelectric panel speaker and the associated experimental arrangement are shown in Figs. 6(a) and (b), respectively.



(a)



(b)

Figure 6. Experimental arrangement of the piezoelectric panel speaker. (a) Physical construction of the piezoelectric panel speaker. (b) The experimental setup for the performance measurement.

The boundary of PC diaphragm is approximated as simply supported. The piezoelectric ceramic plates have been clamped completely onto the surrounding frame.

Response simulation and experimental investigation

A 25 Vrms sweep sine signal is used to drive the speaker, with the frequency varying from 20 Hz to 8 kHz. The on-axis SPL response was measured by a microphone positioned at the center axis with 30 cm away from the speaker. Because of the high input capacitive impedance of the piezoelectric plate, an amplifier capable of supplying high voltage is used. The measured SPL response was compared with the simulation based on Eqs. (23) and (24) in Fig. 7.

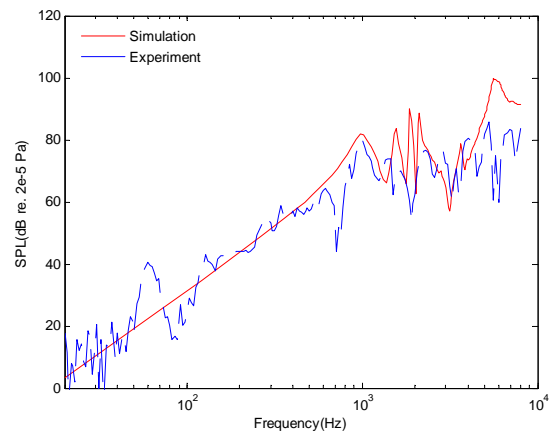


Figure 7. Comparison of the on-axis pressure responses simulated using the FEM and the measurement.

The measurement and the prediction of the speaker responses are in good agreement in terms of the gain level and the fundamental frequency. The discrepancy at the high frequencies could be due to the facts that the selected finite element mesh fails to account for such a high frequency range and the simply supported boundary conditions deviate from real conditions. In addition, inaccuracy of material constants and numerical errors introduced by the shape function interpolation can also contribute to the discrepancies at the high frequency responses.

Optimal design obtained using the SA algorithm

The parameters of annealing schedule for the SA search are summarized in Table 2.

Table 2. The parameter setting of annealing schedule used in the SA optimization procedure.

Parameter	Value
Initial temperature, T_0	10
Initial temperature, T_f	10e-9
Markov chains	4
Temperature reduction rate, α_T	0.85

With this setting, we search for the positions to mount the piezoelectric ceramics that would maximize the ratio of the average SPL to the fundamental frequency. The learning curve of the SA search is shown in Fig. 8.

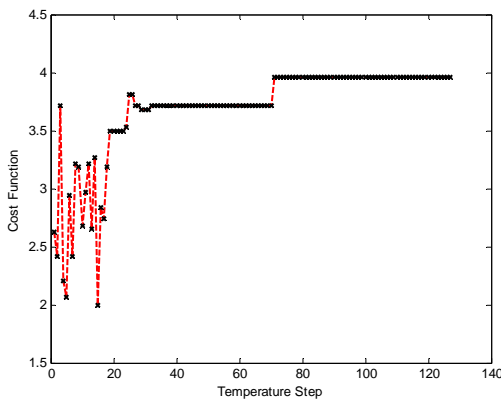


Figure 8. The learning curve of the optimal positions of the piezoelectric ceramic plates. The result has converged in 70 temperature steps (280 iterations).

The cost function has converged to 3.954 after 70 temperature steps (280 iterations). The search pattern of optimal positions of the piezoelectric ceramic plates shown in Fig. 9 has converged from (46, 138) to (42, 124).

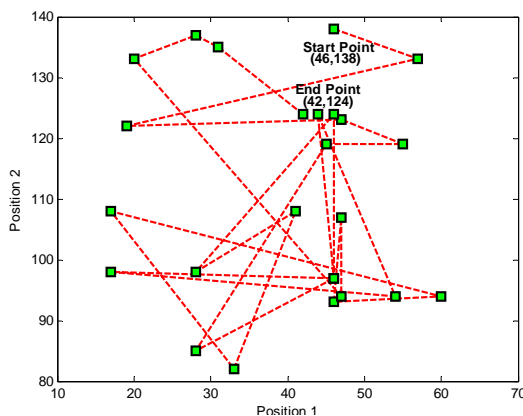


Figure 9. The search history of SA for optimizing positions to mount the piezoelectric ceramic plates.

The optimal positions to mount piezoelectric ceramic plates are at nodes 42 and 124 and physical construction is shown in Fig 10(a) (the node number is defined as the node anchored at the upper left corner of the spacer). Fig. 10(b) compares the SPL responses of the optimal design and a non-optimal design of piezoelectric ceramic plates. The optimal design results in $f_0 = 680$ Hz, $p_{avg} = 82.6$ dB, where the cost function attains 3.95. On the other hand, the non-optimal design with the piezoelectric ceramic plates mounted at node 57 and 96, respectively, results in $f_0 = 980$ Hz, $p_{avg} = 83.25$ dB, where the cost function attains 2.96. The design with the piezoelectric ceramic plates at the optimal positions markedly outperformed the non-optimal design. The fundamental resonance frequency, f_0 , has been reduced with the optimal design by approximately 300 Hz (from 980 Hz of the original design to 680 Hz of the optimal design) with a slight 0.65 dB SPL loss.

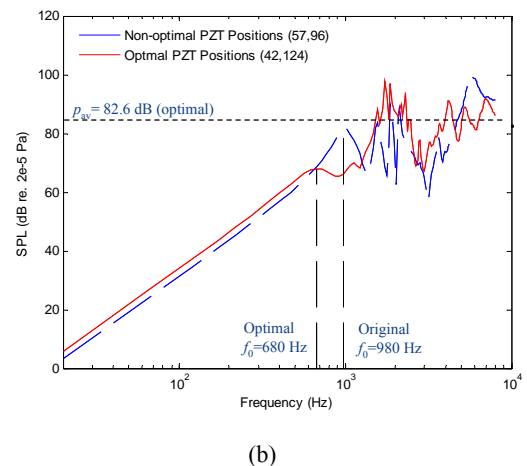
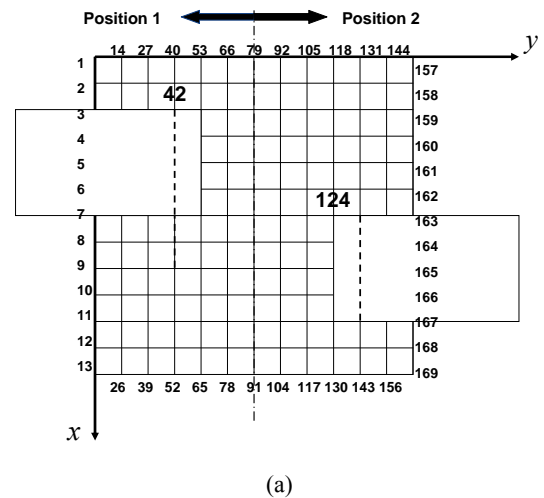


Figure 10. Comparison between the original and the optimal designs of the piezoelectric panel speaker. (a) The optimal positions to mount piezoelectric ceramic plates. (b) On-axis pressure responses.

CONCLUSIONS

A new design of panel speaker driven by two cantilever piezoelectric ceramic plates is presented. A FEM-based model has been developed to establish the simulation platform for response prediction. By taking acoustical loading into account, the FEM model yielded reasonable predictions in line with the experimental results. SA technique is employed to optimize

the positions to mount the piezoelectric ceramic plates such that the fundamental frequency and high average SPL output can be achieved. As evident from the numerical and the experimental results, the optimal configuration had improved the acoustic performance of the piezoelectric panel speaker over the non-optimal design.

ACKNOWLEDGMENTS

The work was supported the National Science Council in Taiwan, under the project number NSC 95-2221-E-009 -009 -MY2.

REFERENCES

- 1 S. S. Iyer, and Haddad, Y. M. Haddad, "Intelligent materials-An overview" *Int. J. of Pressure Vessels and Piping*, **58**, 335-344 (1994).
- 2 G. Bank, N. Harris, and M. Colloms, "Resonant element transducer" *US patent*, 7,149,318 (2006).
- 3 N. Sashida, H. Itoh, S. Ishii, and Y. Watanabe, "Piezoelectric vibrator" *US patent*, 7,247,976 (2007).
- 4 Longbottom, S. A., Matheson, A., McKeivitt, G., Topliss, R., Pitts, M. J. and Shepherd, M. R. Loudspeaker. *US patent*, 7,302,068, 2007.
- 5 S. S. Lee and R. M. White, "Piezoelectric cantilever voltage-to-frequency converter" *Sensors and Actuators A***71**, 153-157 (1998).
- 6 S. E. Woodard, "Method to increase sound quality produced from piezoelectric devices" *J. Sound Vib.* **280**, 127-140 (2005).
- 7 X. C. Chu, X. P. Bi, and L. Li, "Optimization, design and preparation of multi-layers piezoelectric speakers" *The 4th International Workshop on Piezoelectric Materials and Application in Actuators* (2007).
- 8 M. R. Bai and Y. C. Lu, "Optimal implementation of miniature piezoelectric panel speakers using the Taguchi method and genetic algorithm" *ASME/J. Vib. Acoust.* **126**(3), 359-369 (2006).
- 9 M. R. Bai, and B. W. Liu, "Determination of optimal exciter deployment for panel speakers using the genetic algorithm" *J. Sound Vib.* **269**, 727-743 (2004).
- 10 M. R. Bai, and C. H. Huang, "Optimization and implementation of piezoelectric radiators using the genetic algorithm" *J. Acoust. Soc. Am.* **113**(6), 3197-3208 (2003)
- 11 S. Kirkpatrick, C. D. Gelatt, and M. P. Vecchi, "Optimization by Simulated Annealing. *Science*" **220**, 671-680 (1983).
- 12 C. R. Davis, *Concepts and applications of finite element analysis* (J. Wiley and Sons, 1989).
- 13 A. P. Berkhoff, "Sensor Scheme design for active structural acoustic control" *J. Acoust. Soc. Am.* **108**, 1037-1045 (2000).
- 14 L. Meirovitch, *Elements of vibration analysis* (McGraw-Hill, Singapore, 1986).